Published in final edited form as:
NMR Biomed. 2013 November ; 26(11): 1471–1483. doi:10.1002/nbm.2978.

Multiple Echo Diffusion Tensor Acquisition Technique (MEDITATE) on a 3T clinical scanner

Steven H. Baete[1], **Gene Cho**[1,2], and **Eric E. Sigmund**[1]

[1]Bernard and Irene Schwartz Center for Biomedical Imaging, Dept. of Radiology, NYU Langone Medical Center, New York, NY, USA

[2]Sackler Institute of Graduate Biomedical Sciences, NYU School of Medicine, 660 1st Ave, 4th Floor, New York, NY 10016, USA

Abstract

This paper describes the concepts and implementation of an MRI method, Multiple Echo Diffusion Tensor Acquisition Technique (MEDITATE), which is capable of acquiring apparent diffusion tensor maps in two scans on a 3T clinical scanner. In each MEDITATE scan, a set of RF-pulses generates multiple echoes whose amplitudes are diffusion-weighted in both magnitude and direction by a pattern of diffusion gradients. As a result, two scans acquired with different diffusion weighting strengths suffice for accurate estimation of diffusion tensor imaging (DTI)-parameters. The MEDITATE variation presented here expands previous MEDITATE approaches to adapt to the clinical scanner platform, such as exploiting longitudinal magnetization storage to reduce T_2-weighting. Fully segmented multi-shot Cartesian encoding is used for image encoding. MEDITATE was tested on isotropic (agar gel), anisotropic diffusion phantoms (asparagus), and *in vivo* skeletal muscle in healthy volunteers with cardiac-gating. Comparisons of accuracy were performed with standard twice-refocused spin echo (TRSE) DTI in each case and good quantitative agreement was found between diffusion eigenvalues, mean diffusivity, and fractional anisotropy derived from TRSE-DTI and from the MEDITATE sequence. Orientation patterns were correctly reproduced in both isotropic and anisotropic phantoms, and approximately so for *in vivo* imaging. This illustrates that the MEDITATE method of compressed diffusion encoding is feasible on the clinical scanner platform. With future development and employment of appropriate view-sharing image encoding this technique may be used in clinical applications requiring time-sensitive acquisition of DTI parameters such as dynamical DTI in muscle.

Keywords

Diffusion; DTI; Multiple Modulation Multiple Echo; Fast Acquisition

Introduction

Diffusion tensor imaging (DTI) [1, 2] provides biomarkers of tissue anisotropy and microstructure (principal diffusivities (λ_1, λ_2 and λ_3), mean diffusivity (MD) and fractional anisotropy (FA)), which have many applications in oriented biological tissue (e.g. neural fibers [3], renal tubules [4], muscle fibers [5–7]). Typically, the DTI parameters are derived from a set of diffusion-weighted images, most commonly collected with echo-planar imaging (EPI) [8]. Often, each of these images probes diffusion in one direction with one weighting magnitude [9, 10]. The diffusion information encoded in the set of sequential acquisitions is decoded in post-processing in order to estimate a full 3D diffusion tensor.

Corresponding author: Steven Baete, steven.baete@nyumc.org, tel. +1 212 263 4861.

In an alternative approach, several diffusion directions and/or weightings can be sampled in one acquisition [11–13]. Initial work obtained additional diffusion sampling by adding diffusion gradients to a train of refocused gradient and spin echoes [11]. This was later extended in the Difftrain-approach [14], using a stimulated echo rather than a spin echo preparation. Another possible approach is the generation of several echoes which are subsequently refocused, as in a DANTE-preparation [15] and more comprehensively with the Multiple-Modulation-Multiple-Echo (MMME)-approach [12, 16]. A related class of techniques involve multiple diffusion-weighted coherence pathways that are temporally superposed into steady state composite signals [17–19]. Multiple such signals can be acquired for improved efficiency and quantification [20].

The MMME-pulse sequence family, reviewed in [16], employs multiple echoes in one acquisition to quickly measure multiple MR parameters. MMME applications have included fast imaging [21], flow measurement [22, 23] and most notably, diffusion imaging [12, 16, 24–26]. In the latter approach, dubbed MEDITATE for Multiple Echo Diffusion Tensor Acquisition Technique, a pattern of diffusion gradients between the multiple RF-pulses encodes a train of echoes with each echo having a different diffusion weighting and direction. In a pre-clinical setting, the MEDITATE-sequence was shown to estimate full three-dimensional diffusion tensor maps in five encodings [25]. A subsequent non-spatially resolved variant showed that the diffusion tensor can be acquired in two shots [26]. However, translation of the latter to a clinical setting is nontrivial due to hardware and SNR limitations. Most importantly, the lower gradient strengths available in a clinical setting necessarily lengthen the sequence timing. This limits the SNR attainable with the MEDITATE method in materials with a short T_2, a problem which affects the common EPI DTI method less severely.

In this study, we introduce a variation of the MEDITATE sequence, expanding the possibilities of the MMME-pulse sequence family. This method overcomes the limitations of scanner hardware and *in vivo* short T_2-relaxation time (e.g. in muscle tissue [27]) present in previous versions of the MEDITATE sequence, by exploiting longitudinal magnetization decay. Multiple stimulated and spin echoes are diffusion encoded utilizing a MMME magnetization preparation module. The resulting longitudinal magnetization is then read out by a train of pulses. Additional diffusion gradients further add to the diffusion weighting of the echoes and expand their directional sensitivity. The diffusion contrast is isolated from flip angle and relaxation effects via a weighted reference scan. This approach allows an estimation of the apparent 3D diffusion tensor in as few as two acquisitions, one diffusion weighted scan and one reference scan. Multiple diffusion-weighted echo sets with complementary encoding patterns can be included in the inversion if time permits their collection. In the present work, we consider two cases: 2 diffusion-weighted scans and 1 reference scan, and the minimal 1 diffusion-weighted scan and 1 reference scan (referred to herein as the three and two dataset methods). When combined with appropriate k-space trajectories, the compressed diffusion encoding approach may allow time-resolved DTI.

In this paper, we will describe the adaptation of the original MEDITATE-method [16, 25, 26] to the current method (Figure 1a). First, in the Theory section, we will discuss the diffusion weighting encoding and its optimization. Secondly, we will present simulations of the impact of noise and time-dependent diffusion on the apparent diffusion contrast and of the directional variance of MEDITATE. Next, the feasibility and results of the method will be demonstrated in an isotropic phantom, a fibrous phantom, and within *in vivo* human skeletal muscle using a clinical MRI scanner. Finally, in the discussion section, we will summarize results, comment on limitations, and consider future applications of this encoding scheme.

Theory

Coherence pathway formalism

In this paper, we will use the coherence pathway formalism [12,16,28–32], an alternative but formally equivalent notation to the echo pathway description [33, 34], to calculate the echo times, relaxation, and diffusion weighting of each echo in the sequence. In short, the amplitude of each echo in the sequence can be expressed as a product of the total magnetization M_0 with three factors

$$M_Q = M_0 \cdot A_Q \cdot B_Q \cdot C_Q \quad (1)$$

each a function of the coherence pathway Q leading to the echo. Neglecting off-resonance effects, A_Q depends only on the RF-flip angles α_i and phases ϕ_i, B_Q depends on spin relaxation weighting (T_1, T_2) and the time-spacing τ_j between the RF-pulses and C_Q accounts for the diffusion weighting experienced along the coherence pathway

$$C_Q = \exp\left(-\sum_{mn} b_{mn,Q} D_{mn}\right) \quad (2)$$

with D_{mn} the diffusion tensor elements and m and $n = x, y, z$. The diffusion weighting factors $b_{mn,Q}$ can be calculated in the standard way [12,25]

$$b_{mn,Q} = \int_0^{TE_Q} k_{m,Q}(t) k_{n,Q}(t) dt \quad (3)$$

$$k_{m,Q}(t) = \gamma \int_0^t \mu(t') G_m(t') dt', \quad (4)$$

with $\vec{G}$ the gradient waveform including imaging and spoiler gradients, TE_Q the echo formation time and $\mu(t)$ the instantaneous value of the magnetization state of Q (0, +1 or −1 for the three states of spin magnetization of an ensemble of spin-1/2 nuclei $M_0 = M_z$, $M_+ = (M_x + iM_y)/\sqrt{2}$ and $M_- = (M_x - iM_y)/\sqrt{2}$). When choosing the amplitude and timing of diffusion gradients in this method, the echo formation condition expands to [25]

$$\int_0^{TE_Q} \mu(t) \vec{G}(t) dt = 0. \quad (5)$$

Equation (5) needs to be fulfilled for each coherence pathway Q generating a measured echo.

In order to analyze the diffusion effects encoded in the echo amplitudes, C_Q needs to be separated from the nondiffusive elements in Eq. (1) [12,25]. Although the RF- and relaxation factors A_Q and B_Q can be directly calculated when flip angles and relaxation times are known, this approach fails in the presence of B_1-field inhomogeneities. A more robust method [26] acquires a reference experiment $M_{Q,0}$ with low diffusion weighting and identical RF-pulses and timing as the weighted experiment M_Q. As a result the factors A_Q and B_Q in (1), i.e. the effects of spin relaxation (T_1, T_2), RF-flip angles α_i and flip angle inhomogeneities, can be normalized out

$$\frac{M_Q}{M_{Q,0}}=\frac{A_Q\cdot B_Q\cdot C_Q}{A_Q\cdot B_Q\cdot C_{Q,0}}=\frac{C_Q}{C_{Q,0}}=\exp\left(-\sum_{mn}(b_{mn,Q}-b_{mn,Q,0})D_{mn}\right). \quad (6)$$

The RF-pulse flip angles α_i are chosen to minimize variations of the product of the magnetization fraction A_Q and the relaxation weighting B_Q between the coherence pathways. That is, optimal RF-flip angles maximally equalize the analytical expressions of $A_Q \times B_Q$ for all retained echoes, in contrast to earlier work which did not consider the relaxation weighting B_Q in the flip angle optimization [12, 16, 25]. For the 5 RF-pulse sequence (Figure 1a; human muscle T_1 = 1420 ms, T_2 = 32 ms at 3T [27]) the optimal angles are calculated to be 61°-73°-100°-45°-90°.

In previous work on the MEDITATE diffusion sequence [16, 25, 26], it was shown that the full apparent diffusion tensor can be estimated in two shots in a spectroscopic approach [26]. However, the lower gradient strengths available on clinical scanners require longer timing τ_i to achieve the same diffusion weighting. In combination with the low T_2 of e.g. human muscle (muscle T_2 = 32±2 ms at 3T [27]), this proved to be detrimental for the SNR of the latter 9 echoes in the measurement (Figure 2).

Diffusion and spoiler gradients

Here, we introduce a new variation of the MEDITATE method (Figure 1a). This variation discards the coherence pathways which experience long periods of transversal magnetization decay in favor of coherence pathways dominated by longitudinal magnetization decay. That is, the first two RF-pulses generate a set of 4 coherence pathways (Figure 1a), each split by the third RF-pulse into three different pathways. One set of four pathways is refocused and generates echoes 2–5 (Table 1). A second set of four coherence pathways experiences transversal magnetization decay (not plotted in Figure 1a) and when T_2 is short, any future echoes generated from these latter coherence pathways will suffer from low SNR. In contrast, the third set of coherence pathways undergoes longitudinal magnetization decay and is subsequently refocused to generate echoes 6–9 (Table 1). This can be repeated several times to generate a train of echoes, each RF-pulse adding 4 echoes. A similar method retaining all echoes, called stimulated MMME, was suggested earlier by Song et al [12].

The diffusion gradients, on three axes (Figure 1a, checkered and hatched areas), encode the diffusion weighting and direction of each coherence pathway according to Equation (3). The diffusion encoding of each echo is determined by the choice of $3 \times (N+1)$ diffusion gradient amplitudes (G_{1x}, G_{1y}, G_{1z}, G_{2x}, G_{2y}, G_{2z}, …, checkered areas in Figure 1a) where N is the number of RF-pulses. All other gradient lobes (Figure 1a, hatched areas) follow from the coherence pathways (Table 1) and the echo formation condition (Equation (5)) [24,25]. These diffusion gradients comprise $N+1$ three-dimensional encoding vectors $\vec{G_j} = (G_{jx}, G_{jy}, G_{jz})/\|(G_{jx}, G_{jy}, G_{jz})\|$ (Figure 1b). In this pictorial representation, the diffusion gradient vectors $\vec{G_1}$ and $\vec{G_2}$ define a plane in which the normalized diffusion vectors $\nu_{b,Q} = \left(\sqrt{b_{xx,Q}}, \sqrt{b_{yy,Q}}, \sqrt{b_{zz,Q}}\right)/\|\left(\sqrt{b_{xx,Q}}, \sqrt{b_{yy,Q}}, \sqrt{b_{zz,Q}}\right)\|$, an approximate representation of the effective diffusion-weighting direction of each echo [25, 26], are directionally distributed. Indeed, $\vec{G_1}$ and $\vec{G_2}$ encode two diffusion directions in the spin magnetization which form a basis for each group of four echoes. While the representation using the diffusion vectors $\nu_{b,Q}$ is not formally equivalent to that used for more conventional diffusion sampling, this representation gives a useful intuition of the diffusion encoding.

In addition to the diffusion gradient vectors $\vec{G_1}$ and $\vec{G_2}$, a second group of diffusion gradients (Figure 1a, $\vec{G_3}$ to $\overrightarrow{G_{N+1}}$), was added to the sequence. These bipolar gradients,

grouped in diffusion gradient vectors $\vec{G_j} = \left(\vec{G_{jx}}, \vec{G_{jy}}, \vec{G_{jz}}\right)$, add to the diffusion encoding in arbitrary directions. Since the bipolar gradient waveform is self-refocused, they do not disturb the balanced gradient pattern of $\vec{G_1}$ and $\vec{G_2}$. $\vec{G_3}$ impacts all but the first coherence pathway, whilst vectors $\vec{G_4}$ to $\vec{G_{N+1}}$ only change the diffusion encoding of the three coherence pathways, which are transversal at that time and subsequently form echoes. As depicted in Figure 1c, these diffusion gradients help to push the effective diffusion directions out of the plane determined by $\vec{G_1}$ and $\vec{G_2}$ (Figure 1b). They are accommodated by a time τ_G added to each RF-time interval except the first.

In this method, echoes are discarded when they experience long periods of transversal magnetization decay along their coherence pathway. Nevertheless, remainders of these coherence pathways and other free induction decays must be spoiled to prevent interference with desired signals. Spoiler gradients are added before RF-pulses number 4 to N (Figure 1a, speckled areas), to the de- and rephasers of the slice selective gradients of RF-pulses number 2 and 3, and wherever needed to balance the gradients of each coherence pathway [13,35] (Figure 1a, *). Furthermore, potential coincident echoes are minimized by a slight delay added to some of the latter RF-pulse time intervals (e.g. when $N > 4$, $\tau_3 \rightarrow \tau_3 + \frac{1}{4}\tau_1$, when $N > 5$, $\tau_4 \rightarrow \tau_4 + \frac{1}{8}\tau_1$, …). The calculation of the diffusion weighting factors $b_{mn,Q}$ (Equation (3)) is straightforward, and must incorporate the imaging and spoiler gradients [36].

Diffusion gradient pattern optimization

Optimal diffusion sampling schemes, optimization methods and comparison metrics are the subject of much research [8–10, 37, 38] and include some guiding features as geometrical considerations, minimum repulsion energy of the diffusion directions or minimal noise propagation. More recently, diffusion sampling schemes have been devised for higher order tensor fitting or specific applications (e.g. [39, 40]). The MEDITATE method exhibits a more limited flexibility in the choice of diffusion sampling directions than conventional diffusion tensor sequences. Despite this limitation, favorable diffusion sampling schemes can be obtained, as described in this section.

The diffusion tensor elements D_{mn} can be extracted from measurements M_Q and $M_{Q,0}$ (Equation (6)), following the conventional processing. This equation can be written in linear form

$$\vec{m} = B \cdot \vec{D} \quad (7)$$

when considering P echoes and where $\vec{m} = [-\ln(M_Q/M_{Q,0})_1, \ldots, -\ln(M_Q/M_{Q,0})_P]'$, $\vec{D} = [D_{xx}, D_{yy}, D_{zz}, D_{xy}, D_{yz}, D_{xz}]'$ and

$$B = \begin{pmatrix} b_{xx,1} & b_{yy,1} & b_{zz,1} & 2b_{xy,1} & 2b_{yz,1} & 2b_{xz,1} \\ \vdots & \vdots & & & & \vdots \\ b_{xx,P} & b_{yy,P} & b_{zz,P} & 2b_{xy,P} & 2b_{yz,P} & 2b_{xz,P} \end{pmatrix} \quad (8)$$

with each element $b_{mn,Q}$ representing $b_{mn,Q} - b_{mn,Q,0}$. One scalar metric quantifying the quality of the diffusion sampling scheme [8, 9] is the condition number of the matrix B [37] which measures how the relative errors propagate from the observed signals ($\delta\vec{m}$) to the calculated parameters ($\delta\vec{D}$)

$$\|\frac{\delta\vec{m}}{\vec{m}}\| \leq \mathrm{cond}(B)\|\frac{\delta\vec{D}}{\vec{D}}\| \quad (9)$$

as derived from the standard theory of error propagation [8,37], with

$$\mathrm{cond}(B)=\|B\|\,\|B^{-1}\|. \quad (10)$$

Here $\|B\|$ equals the largest singular value of B and B^{-1} may represent the pseudoinverse if B is not a square matrix. In practice, condition numbers for conventional DTI sampling schemes were shown to lie in the range of 1.3 to 2 [8,9,37].

The variables for optimization in the variation of the MEDITATE method are the $3 \times (N+1)$ elements of the diffusion gradient vectors $\vec{G_1}$ to $\overrightarrow{G_{N+1}}$ (Figure 1a, 18 optimization variables for a 5 RF-pulse version of MEDITATE). An extra optimization variable was added to represent the relative amplitude of the gradients in the reference experiment $M_{Q,0}$. The main optimization parameter was the condition number (Equation (10)). In addition, the optimization was constrained by adding penalty terms to the optimization parameter to guide the mean isotropic b-value ([1], $\overline{b_{iso}}=\overline{(b_{xx,Q}+b_{yy,Q}+b_{zz,Q})}$ with $Q = 1..P$) to a preset value, as well as to warrant minimum gradient strengths for the elements of the diffusion gradient vectors. It is clear that in this large parameter space any optimization algorithm will only find local minima. In order to close in on the absolute minimum more seed points are chosen and/or the calculation time is increased. We used a direct search optimization algorithm [41] combined with a mesh adaptive search algorithm [42], as implemented in Matlab (The Mathworks, Natick, MA, USA), to optimize the condition number of the encoding matrix B. In a first step, ~ 500 seed points were tried in short optimizations with high termination tolerance, generating the 50 most promising seed points for a more profound optimization with low termination tolerance in the second step. Although we cannot be sure that the absolute minimum condition number was reached, we conjecture that some of the lower local minima were found as several of the optimizations in the second step returned similar endpoints. For the setup described below the lowest condition numbers found were 4.42 (two dataset method) and 3.77 (three dataset method).

Simulations: Time-dependent diffusion and noise impact

The different echo times in this method can influence the resulting apparent diffusion parameters when the diffusion coefficient is time-dependent, e.g. for restricted diffusion. To estimate the extent of this influence, echo amplitudes, simulated using Equation (2) and the sequence parameters from table 2, were fitted with the signal Equation (7). Input diffusion parameters $D(t)$, used to derive diffusion tensor parameters at each echo time t = TE, are calculated according to the short-time $\sqrt{t}$-expansion [43–45]

$$\lambda_{axial} \simeq \lambda_{axial,0}, \quad \lambda_{rad}(t) \simeq \lambda_{rad,0}\left[1-\frac{S}{Vd}\left(\frac{4\sqrt{\lambda_{rad,0}t}}{3\sqrt{\pi}}-\kappa t\right)\right] \quad (11)$$

with λ_{axial} the primary diffusion eigenvalue and $\lambda_{rad} = (\lambda_2 + \lambda_3)/2$ the radial diffusion value, using male human calf muscle parameters derived from time-dependent MR diffusion measurements [8, 45] (fiber size a 61 μm ($a=\frac{2Vd}{S}$, where $\frac{S}{V}$ is the surface-to-volume ratio and d the dimensionality, 2 for diffusion in a cylinder), membrane permeability κ 20 μm/s, D_0 1.52 μm^2/ms ($D_0 = (\lambda_{axial} + 2\lambda_{rad})/3$) and FA 0.4 (parameters for t = 1s); assuming mono-

exponential T_1 and T_2-relaxation). Similar analysis of an isotropic (water) and an anisotropic medium (asparagus stalks (fiber size a 50μm, κ 0.01 10^{-6} μm/s, D_0 1.9 μm^2/ms, simulation parameters chosen based on asparagus $D(t)$ measurements and consistent with both MRI and microscopic imaging [22,46])) allows for the comparison between time-dependent diffusion $D(t)$ (asparagus stalks) and time-independent diffusion (water).

Simulations were repeated for different SNR-levels with Rician noise added to the echo amplitudes at every iteration. At each SNR-level, 400 samples were generated, the actual SNR was determined, and each sample was fitted individually to Equation (7). The resulting apparent diffusion parameters and their standard deviation across the 400 trials were compared with the diffusion parameters at one diffusion time (Δ = 140 ms, average of the echo times, Table 2).

The apparent diffusion parameters derived from the simulation results are summarized in Figure 3. As the SNR-level decreases, the fitted apparent diffusion parameters deviate from the noiseless results; the FA and λ_{axial} increase and λ_{rad} decreases. Despite this eigenvalue splitting, the MD remains stable at lower SNR levels.

Notwithstanding the range of echo times (Table 2), the fitted apparent diffusion parameters approach the diffusion parameters at Δ = 140 ms with an accuracy depending on the measurement subject. That is, the diffusion parameters are estimated precisely when diffusion is not restricted (water) and SNR is high (water, error of estimate at SNR = 1000, MD: 0%). As the SNR decreases or diffusion time-dependence becomes more pronounced over the time range measured, which occurs more strongly in asparagus stalks (Figure 3c) than in human calf muscle (Figure 3e), the accuracy of the diffusion parameter estimates decreases (error of estimate at SNR = 1000; asparagus, MD: 2.5%, FA: 29%; muscle, MD: 0.06 %, FA: 3%). Hence, depending on the precise nature of the diffusion parameter time dependence, FA and the diffusion eigenvalues might be estimated differently than conventional methods; these simulations suggest that FA might be overestimated. However, we expect that relative differences in scalar DTI metrics between successive measurements acquired with the same protocol will be robust imaging markers for individual or group evaluations.

Simulations: Directional variance

In the MEDITATE sequence, the diffusion encoding directions can not be chosen arbitrarily, rather they are the result of an optimization procedure which also considers timing and maximum gradient strength (see above). As a result, diffusion tensor orientation estimates might be influenced by the diffusion directions selected. The extent of this influence is assessed by computing for each tensor orientation with the 95% cone of uncertainty [47], which is the 95% percentile of the angular deviation between the principal eigenvector of 5000 simulated noisy datasets and their dyadic mean tensor. For these calculations, the tensors (constant MD of 1.5 10^{-9} m^2/s, varying FA and SNR [47]) were rotated using a similarity transform to 660 different orientations uniformly spaced over the hemisphere. The echo amplitudes of each tensor were simulated using Equation (2) and the sequence parameters from table 2; Rician noise was added to 5000 copies of this dataset and the resulting echo amplitudes were fitted with the signal Equation (7). From the estimated (noisy) diffusion tensors, the 95% confidence intervals were calculated [47].

The computed 95% cone of uncertainty values (Figure 4) indicate that the directional variance will increase with decreasing SNR and decreasing FA (Figure 4a) as can be expected. In addition, the confidence angle of the estimated tensor orientation depends on the it's orientation relative to the diffusion gradients, with a better performance along the

main axes (Read θ/ϕ = 0/0, Phase θ/ϕ = 90/0 and Slice θ/ϕ = 0/90) than along the Read = Phase (θ/ϕ = 45/0) and Read = Slice (θ/ϕ = 45/45) directions.

Methods

All images in this work were acquired using a 3T wide-bore Siemens Skyra scanner (Erlangen, Germany) with a 15-channel knee coil (QED, Mayfield Village, OH, USA). For comparison of the accuracy and directional diffusion sensitivity of the MEDITATE-method (not the time efficiency) axial DTI was performed using a Spectral Adiabatic Inversion Recovery (SPAIR) fat-saturated twice refocused spin echo diffusion sequence (TRSE) with echo-planar imaging readout [48] (TR / TE = 7400 ms / 59 ms, 64 × 64 × 5 matrix, 3 × 3 × 10 mm resolution, 6 directions, b = 0,500 s/mm^2, 3 averages, scan time 2:59 min (not optimized for time)).

The MEDITATE-sequences were implemented with a fully segmented Cartesian acquisition scheme, i.e. one k-space line for all echoes was collected per shot. All MEDITATE-acquisitions had a TR of 4000 ms, a 64 × 64 matrix, 3 × 3 mm resolution and a slice thickness of 10 mm (scan time 4:16 min per diffusion gradient set, hence 8:32 min for the two dataset MEDITATE with one weighted and one unweighted dataset). The mean isotropic b-value encoded in the echoes was 450 s/mm^2, in accordance with the literature of *in vivo* skeletal muscle DWI [5–7,49–52]. After optimization, optimal sets of diffusion gradient vector moments $\vec{G_1}$ to $\vec{G_{N+1}}$ (Figure 1a) were found as listed in Table 2. The spoiler gradients (speckled areas and included in other gradients on positions labeled with * in Figure 1) were chosen to generate a dephasing of 50π (speckled areas) and 20π (*) respectively over the slice width (e.g. the moment is $\frac{50\pi}{\gamma\Delta z}$, with Δz the slice thickness). The flip angles α_i were chosen as described above and the RF-timing intervals were (τ_1) - (3 × τ_1 + τ_G) - (4.75 × τ_1 + τ_G) - (4.625 × τ_1 + τ_G) with τ_1 and τ_G as listed in Table 2. The echo time ranges quoted in Table 2 refer to the total time between the first RF pulse and the echo formation time.

The resulting datasets were processed offline in three steps (Matlab, Mathworks). In the first step, a Rician noise-correction algorithm was applied to the diffusion-weighted images [52, 53]. Subsequently, Equation (7) was solved pixelwise to generate maps of diffusion eigenvalues (λ_{axial} and λ_{rad}), MD, FA, and FA-weighted color maps. Finally, the diffusion parameters in regions of interest (ROIs) were evaluated by calculating the average and standard deviation over the ROI. Mean axial diffusion eigenvectors were used to calculate the difference angles between the diffusion directions of the TRSE and MEDITATE DTI estimates.

The 5 RF-pulse MEDITATE sequence was validated in three systems: an isotropic sample (agar gel), an anisotropic phantom (asparagus stalks) and *in vivo* in healthy volunteers. The isotropic sample agar gel was made by dissolving 3.5%(w/w) agar (UltraPure Agarose, Invitrogen, Carlsbad, CA, USA) in tap water (25°C), heating the solution to 80°C and pouring the slightly cooled solution (55°C) into a plastic container. Asparagus stalks have been shown [24,25,46] to exhibit diffusion anisotropy in accordance to their prolate cell structure. More precisely, diffusion along the stalk is approximately 30% larger than transverse to the stalk. In this work, asparagus stalks (fresh from a local grocery store; Organic produce from Peru) were submerged in tap water (1h), after which they were cut to length, and stacked in three directions in a plastic container. The voids were filled with agar gel.

The levels of the right calves with the largest cross-sectional area of five healthy volunteers (3 male and 2 female, age 33.0 ± 3.4 y/o) were scanned under a research protocol approved

by the local institutional review board. For the *in vivo* scan, frequency selective fat saturation was used and the acquisition was triggered using ECG gating (trigger delay of 600ms from the R-wave) [54]. The latter increased the scan time from 4:16 to approximately 5:30 per diffusion gradient set in a subject-specific manner. Regions of interest were manually drawn on both TRSE and MEDITATE images enclosing the anterior tibialis (AT), the posterior tibialis (PT) and gastrocnemius medialis (GM) compartments. Results of DTI metrics were averaged over these ROIs for each subject. The mean and standard deviation of these values across all 5 subjects was computed for each sequence.

Results

Figure 5 shows the normalized agar gel signal amplitude of the latter 13 echoes of a two-scan 5 RF-pulse MEDITATE sequence as a function of the full diffusion weighting argument, demonstrating the quality of the fit estimating the diffusion tensor $\vec{D}$.

The raw images in Figure 6 were acquired with the two-scan 5 RF-pulse MEDITATE sequence (Table 2). In these images, magnitude variations include effects from diffusion, RF pulse flip angles, and relaxation. The effect of relaxation on the signal magnitude can be seen in the stronger T_2 weighting for the in-plane stalks perpendicular to the main magnetic field. These effects are eliminated by forming ratio images, which reflect diffusion contrast alone (Figure 6c).

Diffusion-weighted images such as in Figure 6 were analyzed pixelwise with Equation (7). Examples of this DTI-analysis are plotted in Figure 7 which gives an overview of DTI parameter maps as estimated by the conventional TRSE-DTI and 5 RF-pulse MEDITATE-sequences (Table 2). Figure 7 depicts estimated diffusion parameter maps of an isotropic phantom (agar gel), an anisotropic phantom (asparagus stalks) and *in vivo* calf muscle. ROI analysis of these estimated diffusion parameter maps are plotted in Figure 9, while Figure 8 visualizes the diffusion tensors of the anisotropic phantom with ellipsoidal glyphs (Matlab, fanDTasia toolbox [55]).

Figures 7, 8 and 9 illustrate the agreement between the diffusion tensor parameters estimated with MEDITATE and TRSE-DTI. In the isotropic agar gel (Figure 7a and Figures 9a and 9b), the diffusion eigenvalues are homogeneously high and the FA homogeneously low as expected. The asparagus samples (Figure 7b and Figures 9c, 9d) exhibit λ_{axial}, λ_{radial} and FA values in approximate agreement with earlier work [25] for both sequences. Additionally, the asparagus stalk directivity (horizontal, diagonal, or perpendicular to the image plane) is correctly identified in all segments (Figure 9e), however, less accurately in the diagonal direction due to the increased directional variance (Figure 4). In comparison with the diffusion eigenvalues of TRSE-DTI, the diffusion eigenvalues of the asparagus stalks derived from MEDITATE are slightly lower (Figure 9c, λ_{axial} −10.2%, λ_{rad} −31.7%), a consequence of the longer diffusion time in the MEDITATE sequence. In general, the asparagus diffusion parameter estimates are relatively robust for the variations of the MEDITATE-sequences tested.

The mean diffusion eigenvalues in the *in vivo* calf muscle estimated with the 3 and 2 dataset MEDITATE-sequences are, lower (Figure 9f, λ_{axial} −10.8%, λ_{rad} −10.2%) and higher (Figure 9f, λ_{axial} +20.0%, λ_{rad} −4.2%), respectively, than that of the TRSE-DTI sequence. In addition, the FA is higher in the 2 dataset MEDITATE muscle results, possibly due in part to a residual ghosting artifact in the segmented Cartesian imaging trajectory which is not fully suppressed by the cardiac gating, and in part to higher variance from the higher condition number. However, overall, the estimated diffusion parameters are robust and similar to those found in the conventional TRSE-EPI sequence.

Discussion

In this paper, we present an MRI sequence capable of acquiring apparent diffusion tensor maps in two scans. This method, an adaptation of the MEDITATE-method [12, 24–26], employs a series of diffusion gradients to modulate several echoes with diffusion weighting in both magnitude and direction (Figure 1). Figures 7 and 9 illustrate the capability of MEDITATE to estimate DTI parameters with just three or two encodings. This is a significant compression in diffusion encoding in comparison with more common DTI schemes, which acquire separate scans for at least 6 diffusion encodings and a reference scan,albeit with a faster image encoding.

The diffusion gradient vectors $\vec{G_3}$ to $\overrightarrow{G_{N-1}}$ introduced in the MEDITATE sequence increase flexibility in the directional sensitivity of the diffusion weighting. Their impact on the diffusion encoding directivity can be intuitively understood from the pictorial representations of the normalized diffusion vectors in Figures 1b and 1c. In a slightly different approach, the bipolar gradients ($\vec{G_3}$ to $\overrightarrow{G_{N-1}}$) can be replaced by monopolar diffusion gradients, adjusting all subsequent diffusion gradients according to the echo formation condition (Equation (5)).

It is interesting to note that, in the MEDITATE sequence family, the diffusion time is not well defined [12]. In the more uniform case of a multiple pulsed gradient spin echo (PGSE), Fordham et al. [56] succeeded in deriving an effective diffusion time. Although an effective diffusion time can be derived for each individual coherence pathway [57], the specific multiple echo structure of the MEDITATE sequence prohibits the definition of a single effective diffusion time. Notwithstanding the lack of well defined diffusion time, the diffusion weighting and direction encoded in each echo are determined very precisely by the diffusion weighting factors (Equation (3)); this information suffices for DTI analysis within the Gaussian diffusion tensor approximation.

In the case of samples with a time-dependent diffusion coefficient $D(t)$, the MEDITATE-sequence has been shown to overestimate [26] or underestimate (Figure 3) the mean diffusivity. Although no diffusion time is defined in this paper for each echo in the MEDITATE sequence, it is clear that each echo will sample a different portion of $D(t)$. This might limit the accuracy of the estimation of diffusion parameters with the MEDITATE sequence [25, 43, 58]. Computer simulations (Figure 3) suggest that the extent of this effect depends on the precise nature of $D(t)$ relative to the diffusion gradient pattern and sequence timing with a larger effect as diffusion time-dependence is more pronounced over the time range measured. At the same time, the computer simulations show that the effect is limited for the systems considered in this study, and that it can possibly be further reduced by incorporating a model for the tissue under study in the optimizations of the diffusion gradient sets. The 2 dataset MEDITATE-sequence underestimates most of the eigenvalues of the measurements with restricted time-dependent diffusion compared to the TRSE-sequence (Figures 9c and 9f). This underestimation relative to the TRSE-sequence stems largely from the difference in diffusion times (TRSE TE = 59 ms, mean MEDITATE TE = 148.2 ms). Simultaneously, computer simulations of the MEDITATE sequence (Figure 3) predict an increased FA and eigenvalue splitting at the measurement SNR levels (asparagus SNR 28.24, *in vivo* male calf muscle SNR 13.34). An alternative approach might take diffusion time dependence into account with an explicit model in the MEDITATE tensor inversion, but the assumptions and optimizations of such a strategy have not yet been explored.

The DTI parameter estimates obtained with the MEDITATE-method (Figure 9) are fairly robust in spite of a number of limitations. While the differences in magnetization fractions and relaxation weightings are eliminated by the reference experiment (Equation 6) and the differences in diffusion weighting are accounted for by the precise calculation of the diffusion weighting factors (Equation 3), a possible limitation is that some echoes are stimulated echoes and some echoes are spin echoes. Correspondingly, all echoes experience different periods of transverse and longitudinal relaxation. Thus, local magnetic field deviations originating e.g. in magnetic susceptibility differences, might influence the diffusion weighting of the echoes differently. Similarly, for systems like skeletal muscle whose compartmental complexity gives rise to multi-exponential relaxation, the relative importance of the components might vary amongst echoes and thus affect quantification [14]. Further, the MEDITATE analysis assumes Gaussian diffusion behavior and uses b-values within that regime; higher order models (Intravoxel Incoherent Motion (IVIM) [59], Diffusional Kurtosis Imaging (DKI) [60], q-space [61]) are not considered. Likewise, as mentioned above, time-dependent diffusion is not explicitly accounted for in the tensor inversion. Finally, although the echoes display different SNR, no weighting factors were applied in the analysis.

An additional possible limitation of the MEDITATE-method is the resemblance to double wave vector (DWV) experiments [62, 63]. In such DWV experiments, two consecutive PGSE blocks, each with a pair of diffusion gradients, are intended to probe microscopic anisotropy and/or pore ellipticity, where the single PGSE lacks sensitivity [62, 63]. Hence, also the MEDITATE sequence could be susceptible to pore shape and size sensitivities. However, since the sequence was not designed to this end, it does not readily lend itself to the existing formalism. In addition, in the low-q regime, the Gaussian component of the diffusion is the dominating factor. Moreover, as the departure from the underlying Gaussian assumption in the time-dependent diffusion has a limited effect on the DTI estimates, and given formal relationships between this time-dependence and some of the restriction-induced angular modulation inherent to DWV contrast [64], it is conjectured that also the DWV-effects originating from compartment size will have a limited effect on the DTI estimates; i.e. the MEDITATE sequence supplies a fairly robust though approximate estimate of the DTI parameters. However, a full study of the DWV-effects in MEDITATE is beyond the scope of this paper.

The segmented Cartesian sampling scheme used in this implementation of the MEDITATE-method is sensitive to ghosting in the phase encoding direction for the *in vivo* muscle acquisitions due to motion and cardiac pulsatility of the skeletal musculature [65]. Even though ECG triggering was used to minimize the cardiac pulsatility for the *in vivo* scans, minimal ghosting could be seen in the raw images. This effect might partially explain the deviations in the estimated *in vivo* eigenvalues and the higher anisotropy in the *in vivo* scans (Figures 7 and 9).

The two acquisition 5 RF-pulse MEDITATE sequence significantly compresses the diffusion encoding in comparison to standard DTI acquisition schemes. That is, MEDITATE acquires 13 diffusion encodings of a k-space line in two repetitions where standard DTI acquisition schemes sense one diffusion encoding of the whole k-space per repetition. However, the compressed diffusion encoding has thus far been developed independently from the image encoding scheme, which means that the MEDITATE sequence, with the current segmented Cartesian image encoding, has a lower imaging efficiency than the TRSE sequence (e.g. *in vivo* SNR = 34.0 versus 54.5 and imaging efficiency γ = 1.07 versus 4.42, with $\gamma = (\mathrm{SNR/voxel})/\sqrt{T_T}$, T_T the total acquisition time [34]). To reduce the overall scan time in a spatially resolved approach, the suggested compressed diffusion encoding can be

combined with an appropriate k-space trajectory, e.g. a radial sampling scheme [66–68]. When also including self-navigation with phase corrections [66,68] and view-sharing [69,70], this sequence may potentially allow time-resolved DTI acquisition in dynamic systems such as mobile skeletal muscle.

The diffusion gradient vector sets for the MEDITATE-sequence (Table 2) constitute diffusion encoding schemes sufficient for 3D DTI. Calculations of the 95% cone of uncertainty (Figure 4) illustrate that the directional variance of the MEDITATE diffusion encoding scheme is higher than e.g. the 6 direction dual-gradient sampling scheme of the TRSE sequence [47]. However, this is mainly problematic in specific tensor directions, e.g. the diagonal direction in the asparagus phantom (Figures 7b and 8b). Whilst the optimization of the diffusion gradient vector sets aimed for a low condition number, additional scalar optimization indices can be considered, such as rotational invariance [38] or minimal DTI parameter variance in a sample set of directions (e.g. [10, 39, 40]). The latter approach could reduce the direction variance of the diffusion sampling and also allow for specialized diffusion sampling optimized for prior knowledge.

In conclusion, we presented an MRI method which compresses the diffusion encoding for DTI. This MRI method is capable of acquiring apparent diffusion tensor maps in two scans, utilizing a slow segmented Cartesian image encoding scheme. The compression of the diffusion encoding is accomplished by modulating multiple echoes, generated by a train of RF-pulses, with diffusion weighting in both magnitude and direction by a pattern of diffusion gradients. The presented MRI sequence is an adaptation of earlier work, limited by low SNR in systems with low T_2, on the Multiple Echo Diffusion Tensor Acquisition Technique (MEDITATE). MEDITATE is adapted here to exploit the longer longitudinal magnetization storage and additional diffusion gradients are added to allow the necessary flexibility in the directional sensitivity of the diffusion weighting. The method is demonstrated in an isotropic phantom, an anisotropic fibrous phantom and within *in vivo* human skeletal muscle. With future development, this technique may be used in clinical applications requiring time-sensitive acquisition of DTI parameters such as dynamical DTI in muscle.

Acknowledgments

This project is supported by NIH (R21EB009435) and by a Fellowship of the Belgian American Educational Foundation. We thank the NYU Information Technology Services for High Performance Computing (HPC) resources.

Sponsers: National Institutes of health (R21EB009435-01A1) and a Fellowship of the Belgian American Educational Foundation

Abbreviations

MEDITATE	Multiple Echo Diffusion Tensor Acquisition Technique
MMME	Multiple-Modulation-Multiple-Echo
PGSE	Pulsed Gradient Spin Echo
TRSE	twice-refocused spin echo
DTI	Diffusion Tensor Imaging
DWI	Diffusion Weighted Imaging
MD	Mean diffusivity

FA	Fractional Anisotropy
EPI	Echo-planar Imaging
DWV	Double Wave Vector
SNR	Signal to Noise Ratio
ROI	Region Of Interest

References

1. Basser PJ, Mattiello D. Estimation of the Effective Self-Diffusion Tensor from the NMR Spin Echo. J Magn Reson B. 1994; 103:247–254. [PubMed: 8019776]
2. Alexander AL, Hasan K, Kindlmann G, Parker DL, Tsuruda JS. A Geometric Analysis of Diffusion Tensor Measurements of the Human Brain. Magn Reson Med. 2000; 44:283–291. [PubMed: 10918328]
3. Sundgren PC, Dong Q, Gomez-Hassan D, Mukherji SK, Maly P, Welsh R. Diffusion tensor imaging of the brain: review of clinical applications. Neuroradiology. 2004; 46:339–50. [PubMed: 15103435]
4. Riess M, Jones RA, Basseau F, Moonen CTW, Grenier N. Diffusion Tensor MRI of the Human Kidney. J Magn Reson Imaging. 2001; 14:42–49. [PubMed: 11436213]
5. Damon BM, Ding Z, Anderson AW, Freyer AS, Gore JC. Validation of diffusion tensor MRI-based muscle fiber tracking. Magn Reson Med. 2002; 48:97–104. [PubMed: 12111936]
6. Galban CJ, Maderwald S, Uffmann K, Greiff A, Ladd ME. Diffusive sensitivity to muscle architecture: a magnetic resonance diffusion tensor imaging study of the human calf. Eur J Appl Physiol. 2004; 93:253–62. [PubMed: 15322853]
7. Sinha S, Sinha U. Reproducibility analysis of diffusion tensor indices and fiber architecture of human calf muscles in vivo at 1. 5 Tesla in neutral and plantarflexed ankle positions at rest. J Magn Reson Imaging. 2011; 34:107–19. [PubMed: 21608064]
8. Jones, DK. Diffusion MRI - Theory, Methods, and Applications. Oxford: Oxford University Press; 2010.
9. Hasan KM, Larker DL, Alexander AL. Comparison of Gradient Encoding Schemes for Diffusion-Tensor MRI. J Magn Reson Imaging. 2001; 13:769–780. [PubMed: 11329200]
10. Alexander DC. A general framework for experiment design in diffusion MRI and its application in measuring direct tissue-microstructure features. Magn Reson Med. 2008; 60:439–48. [PubMed: 18666109]
11. Gulani V, Iwamoto GA, Jiang H, Shimony JS, Webb AG, Lauterbur PC. A Multiple Echo Pulse Sequence for Diffusion Tensor Imaging and Its Application in Excised Rat Spinal Cords. Magn Reson Med. 1997; 38:868–873. [PubMed: 9402185]
12. Song YQ, Tang X. A one-shot method for measurement of diffusion. J Magn Reson. 2004; 170:136–48. [PubMed: 15324767]
13. Ong H, Chin CL, Wehrli SL, Tang X, Wehrli FW. A new approach for simultaneous measurement of ADC and T2 from echoes generated via multiple coherence transfer pathways. J Magn Reson. 2005; 173:153–9. [PubMed: 15705523]
14. Stamps JP, Ottink B, Visser JM, Duynhoven JP, Hulst R. Difftrain: a novel approach to a true spectroscopic single-scan diffusion measurement. J Magn Reson. 2001; 151:28–31. [PubMed: 11444933]
15. Doran SJ, Decorps M. A Robust, Single-Shot Method for Measuring Diffusion Coefficients Using the Burst Sequence. J Magn Reson A. 1995; 117:311–316.
16. Sigmund EE, Cho H, Song Y-Q. Multiple-modulation-multiple-echo magnetic resonance. Concepts in Magnetic Resonance Part A. 2007; 30A:358–377.
17. Buxton RB. The Diffusion Sensitivity of Fast Steady-State Free Precession Imaging. Magn Reson Med. 1993; 29:235–243. [PubMed: 8429788]

18. Miller KL, Pauly JM. Nonlinear phase correction for navigated diffusion imaging. Magn Reson Med. 2003; 50:343–53. [PubMed: 12876711]
19. McNab JA, Miller KL. Steady-state diffusion-weighted imaging: theory, acquisition and analysis. NMR Biomed. 2010; 23:781–93. [PubMed: 20886565]
20. Bieri O, Ganter C, Scheffler K. Quantitative in vivo diffusion imaging of cartilage using double echo steady-state free precession. Magn Reson Med. 2012; 68:720–9. [PubMed: 22161749]
21. Cho H, Chavez L, Sigmund EE, Madio DP, Song Y-Q. Fast imaging with the MMME sequence. J Magn Reson. 2006; 180:18–28. [PubMed: 16427794]
22. Cho H, Ren XH, Sigmund EE, Song YQ. A single-scan method for measuring flow along an arbitrary direction. J Magn Reson. 2007; 186:11–6. [PubMed: 17280845]
23. Raguin LG, Ciobanu L. Multiple echo NMR velocimetry: fast and localized measurements of steady and pulsatile flows in small channels. J Magn Reson. 2007; 184:337–43. [PubMed: 17112754]
24. Tang X-P, Sigmund EE, Song U-Q. Simultaneous Measurement of Diffusion along Multiple Directions. J Am Chem Soc. 2004; 126:16336–7. [PubMed: 15600331]
25. Sigmund EE, Song YQ. Multiple echo diffusion tensor acquisition technique. Magn Reson Imaging. 2006; 24:7–18. [PubMed: 16410173]
26. Cho H, Ren XH, Sigmund EE, Song YQ. Rapid measurement of three-dimensional diffusion tensor. J Chem Phys. 2007; 126:154501. [PubMed: 17461641]
27. Gold GE, Han E, Stainsby JA, Wright G, Brittain J, Beaulieu C. Musculoskeletal MRI at 3. 0T: Relaxation Times and Image Contrast. Am J Radiol. 2004; 183:343–351.
28. Kaiser R, Bartholdi E, Ernst RR. Diffusion and field-gradient effects in NMR Fourier spectroscopy. J Chem Phys. 1974; 60:2966.
29. Counsell CJR. Preview: A New Ultrafast Imaging Sequence Requiring Minimal Gradient Switching. Magn Reson Imaging. 1993; 11:603–616. [PubMed: 8345774]
30. Sodickson AA, Cory DG. A generalized k-space formalism for treating the spatial aspects of a variety of NMR experiments. Prog Nucl Magn Reson Spectr. 1998; 33:77–108.
31. Hurlimann MD, Griffin DD. Spin dynamics of Carr-Purcell-Meiboom-Gill-like sequences in grossly inhomogeneous B(0) and B(1) fields and application to NMR well logging. J Magn Reson. 2000; 143:120–35. [PubMed: 10698653]
32. Hurlimann MD. Diffusion and relaxation effects in general stray field NMR experiments. J Magn Reson. 2001; 148:367–78. [PubMed: 11237644]
33. Hennig J. Multiecho Imaging Sequences with Low Refocusing Flip Angles. JMR. 1988; 78:397–407.
34. Haacke, EM.; Brown, RW.; Thompson, MR.; Venkatesan, R. Magnetic Resonance Imaging: Physical Principles and Sequence Design. New York: Springer-Verlag; 1999.
35. Bernstein, MA.; King, KF.; Zhou, XJ. Handbook of MRI Pulse Sequences. Burlington, MA: Elsevier; 2005.
36. Mattiello J, Basser PJ, Le Bihan D. The b Matrix in Diffusion Tensor Echo-Planar Imaging. Magn Reson Med. 1997; 37:292–300. [PubMed: 9001155]
37. Skare S, Hedehus M, Moseley ME, Li T-Q. Condition number as a measure of noise performance of diffusion tensor data acquisition schemes with MRI. J Magn Reson. 2000; 147:340–52. [PubMed: 11097823]
38. Batchelor PG, Atkinson D, Hill DL, Calamante F, Connelly A. Anisotropic noise propagation in diffusion tensor MRI sampling schemes. Magn Reson Med. 2003; 49:1143–51. [PubMed: 12768593]
39. Poot DHJ, Dekker AJ, Achten E, Verhoye M, Sijbers J. Optimal Experimental Designn for Diffusion Kurtosis Imaging. IEEE Trans Med Img. 2010; 29:819–829.
40. Majumdar S, Zhu DC, Udpa SS, Raguin LG. A diffusion gradient optimization framework for spinal cord diffusion tensor imaging. Magn Reson Imaging. 2011; 29:789–804. [PubMed: 21550745]
41. Hooke R, Jeeves TA. Direct Search Solution of Numerical and Statistical Problems. J Ass Comput Mach. 1961; 8:212–29.

42. Audet C, Dennis JE. Mesh Adaptive Direct Search Algorithms for Constrained Optimization. SIAM Journal on Optimization. 2006; 17:188–217.
43. Sen PN. Time-dependent diffusion coefficient as a probe of the permeability of the pore wall. J Chem Phys. 2003; 119:9871.
44. Novikov DS, Fieremans E, Jensen JH, Helpern JA. Random walks with barriers. Nature Physics. 2011; 7:508–514.
45. Fieremans, E.; Novikov, DS.; Sigmund, EE.; Liu, K.; Jensen, JH.; Helpern, JA. In Vivo Measurement of Membrane Permeability and Fiber Size in Calf Muscle Using Time-dependent DWI in. Proc Intl Soc Magn Reson Med; Montreal, Canada. 2011. p. 1153
46. Boujraf S, Luypaert R, Eisendrath H, Osteaux M. Echo planar magnetic resonance imaging of anisotropic diffusion in asparagus stems. MAGMA. 2001; 13:82–90. [PubMed: 11502422]
47. Jones DK. The effect of gradient sampling schemes on measures derived from diffusion tensor MRI: a Monte Carlo study. Magn Reson Med. 2004; 51:807–15. [PubMed: 15065255]
48. Reese TG, Heid O, Weisskoff RM, Wedeen VJ. Reduction of eddy-current-induced distortion in diffusion MRI using a twice-refocused spin echo. Magn Reson Med. 2003; 49:177–82. [PubMed: 12509835]
49. Karampinos DC, King KF, Sutton BP, Georgiadis JG. Myofiber ellipticity as an explanation for transverse asymmetry of skeletal muscle diffusion MRI in vivo signal. Ann Biomed Eng. 2009; 37:2532–46. [PubMed: 19763830]
50. Heemskerk AM, Sinha TK, Wilson KJ, Ding Z, Damon BM. Quantitative assessment of DTI-based muscle fiber tracking and optimal tracking parameters. Magn Reson Med. 2009; 61:467–72. [PubMed: 19161166]
51. Yanagisawa O, Kurihara T, Kobayashi N, Fukubayashi T. Strenuous resistance exercise effects on magnetic resonance diffusion parameters and muscle-tendon function in human skeletal muscle. J Magn Reson Imaging. 2011; 34:887–94. [PubMed: 21769968]
52. Froeling M, Nederveen AJ, Heijtel DF, et al. Diffusion-tensor MRI reveals the complex muscle architecture of the human forearm. J Magn Reson Imaging. 2012; 36:237–48. [PubMed: 22334539]
53. Aja-Fernandez S, Niethammer M, Kubicki M, Shenton ME, Westin C-F. Restoration of DWI Data Using a Rician LMMSE Estimator. IEEE Trans Med Img. 2008; 27:1389–1403.
54. Karampinos, DC.; King, KF.; Sutton, BP.; Georgiadis, JG. In vivo study of cross-sectional skeletal muscle fiber asymmetry with diffusion-weighted MRI in. Conf Proc IEEE Eng Med Biol Soc; Lyon, France. 2007. p. 327-30.
55. Barmpoutis BC, Shepherd TM, Forder JR. Tensor Splines for Interpolation and Approximation of DT-MRI With Applications to Segmentation of Isolated Rat Hippocampi. IEEE Trans Med Img. 2007; 26:1537–1546.
56. Fordham EJ, Mitra PP, Latour LL. Effective Diffusion Times in Multiple-Pulse PFG Diffusion Measurements in Porous Media. J Magn Reson A. 1996; 121:187–192.
57. Zielinski LJ, Hurlimann MD. Short-time restricted diffusion in a static gradient and the attenuation of individual coherence pathways. J Magn Reson. 2004; 171:107–17. [PubMed: 15504688]
58. Sen PN. Time-dependent diffusion coefficient as a probe of geometry. Concepts in Magnetic Resonance. 2004; 23A:1–21.
59. Le Bihan D, Turner R. Intravoxel Incoherent Motion Imaging Using Spin Echoes. Magn Reson Med. 1991; 19:221–227. [PubMed: 1881307]
60. Jensen JH, Helpern JA, Ramani A, Lu H, Kaczynski K. Diffusional kurtosis imaging: the quantification of non-gaussian water diffusion by means of magnetic resonance imaging. Magn Reson Med. 2005; 53:1432–40. [PubMed: 15906300]
61. Cohen Y, Assaf Y. High b-value q-space analyzed diffusion-weighted MRS and MRI in neuronal tissues - a technical review. NMR Biomed. 2002; 15:516–42. [PubMed: 12489099]
62. Mitra PP. Muliple wave-vector extensions of the NMR pulsed-field-gradient spin-echo diffusion measurement. Phys Rev B. 1995; 51:15074–15078.
63. Shemesh N, Ozarslan E, Komlosh ME, Basser PJ, Cohen Y. From single-pulsed field gradient to double-pulsed field gradient MR: gleaning new microstructural information and developing new forms of contrast in MRI. NMR Biomed. 2010; 23:757–80. [PubMed: 20690130]

64. Jespersen SN. Equivalence of double and single wave vector diffusion contrast at low diffusion weighting. NMR Biomed. 2012; 25:813–8. [PubMed: 22134913]

65. Anderson AW, Gore JC. Analysis and Correction of Motion Artifacts in Diffusion Weighted Imaging. Magn Reson Med. 1994; 32:379–387. [PubMed: 7984070]

66. Pipe JG, Farthing VG, Forbes KP. Multishot diffusion-weighted FSE using PROPELLER MRI. Magn Reson Med. 2002; 47:42–52. [PubMed: 11754441]

67. Liu C, Moseley ME, Bammer R. Simultaneous phase correction and SENSE reconstruction for navigated multi-shot DWI with non-cartesian k-space sampling. Magn Reson Med. 2005; 54:1412–22. [PubMed: 16276497]

68. Jiang Y, Hsu EW. Accelerating MR diffusion tensor imaging via filtered reduced-encoding projection-reconstruction. Magn Reson Med. 2005; 53:93–102. [PubMed: 15690507]

69. Madore B, Glover GH, Pelc NJ. Unaliasing by Fourier-Encoding the Overlaps Using the Temporal Dimension (UNFOLD), Applied to Cardiac Imaging and fMRI. Magn Reson Med. 1999; 42:813–828. [PubMed: 10542340]

70. Mistretta CA, Wieben O, Velikina J, et al. Highly constrained backprojection for time-resolved MRI. Magn Reson Med. 2006; 55:30–40. [PubMed: 16342275]

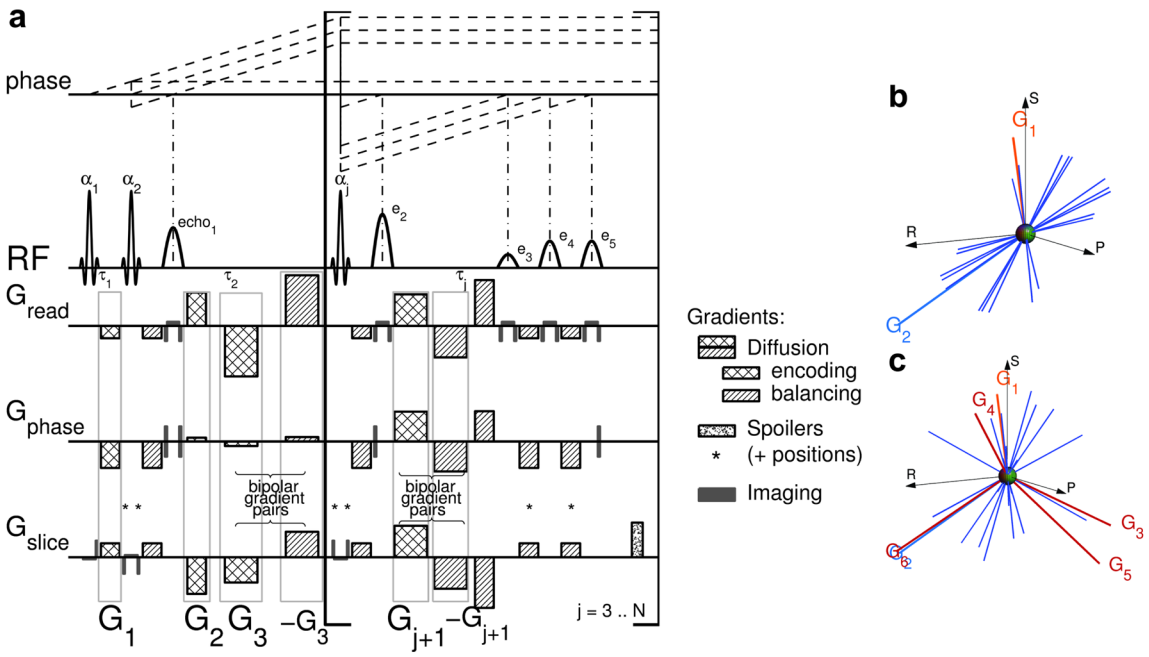

Figure 1.

MEDITATE diffusion tensor acquisition technique. a) The N sinc-shaped slice selective RF-pulses with flip angles α_j separated by time constants τ_j generate a series of $(N-2) \times 4 + 1$ separate echoes, according to the plotted coherence pathways (dashed lines, only reflecting RF induced phase changes and only including eventually refocused echoes). Each of these echoes carries a different diffusion weighting and direction, as encoded by the diffusion gradient vectors $\vec{G_j}, j = 1..(N+1)$ (checkered areas) and their associated rebalancing gradients (hatched areas). Spoiler gradients (speckled areas and included in other gradients on positions labeled *) spoil the remainders of the not retained coherence pathways. (The gradient areas reflect the actual gradient moments whose durations along different physical axes are slightly unequal to minimize slew rate gradient stimulation effects.) b,c) Visual representation of the gradient vectors and the normalized diffusion directions (blue lines, $\nu_{b,Q} = (\sqrt{b_{xx,Q}}, \sqrt{b_{yy,Q}}, \sqrt{b_{zz,Q}}) / \| (\sqrt{b_{xx,Q}}, \sqrt{b_{yy,Q}}, \sqrt{b_{zz,Q}}) \|$ [25,26]) encoded by only $\vec{G_1}$ and $\vec{G_2}$ (b) and by all diffusion gradients $\vec{G_j}, j = 1..(N+1)$ (c). In (b), the diffusion directions populate a single plane determined by $\vec{G_1}$ and $\vec{G_2}$, gradients $\vec{G_j}, j = 3..(N+1)$ push the diffusion directions out of this plane (c) in order to sample all diffusion directions.

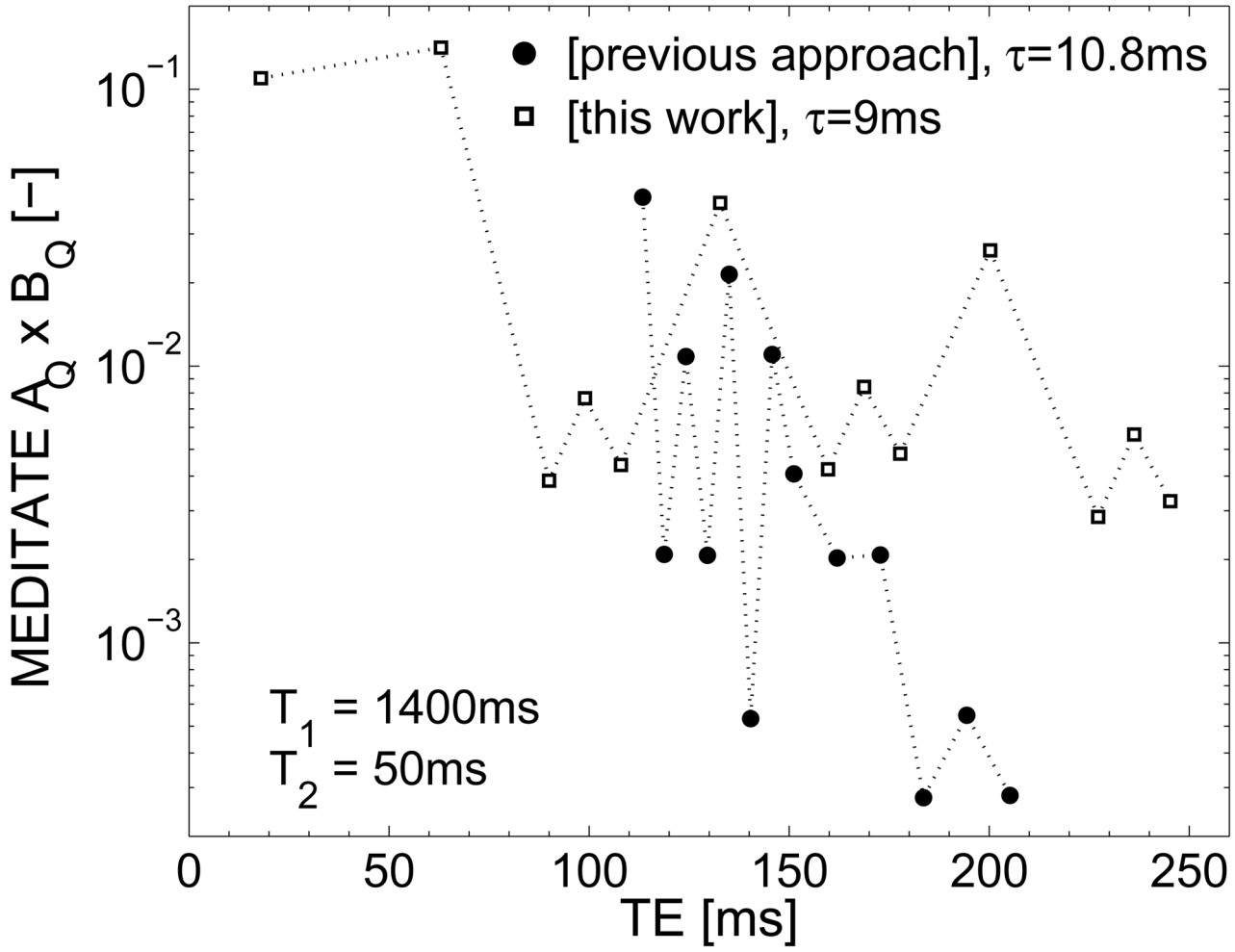

Figure 2.

The magnetization fraction remaining after relaxation effects $A_Q \times B_Q$ (Equation (1), T_1 = 1400 ms and T_2 = 50 ms) of each echo of the previous version [16, 25, 26] and the new variation (with 5 RF-pulses, figure 1a) of the MEDITATE sequence, using typical timing schemes. By utilizing longitudinal magnetization storage, more magnetization is retained in the latter echoes of the MEDITATE variation presented in this work.

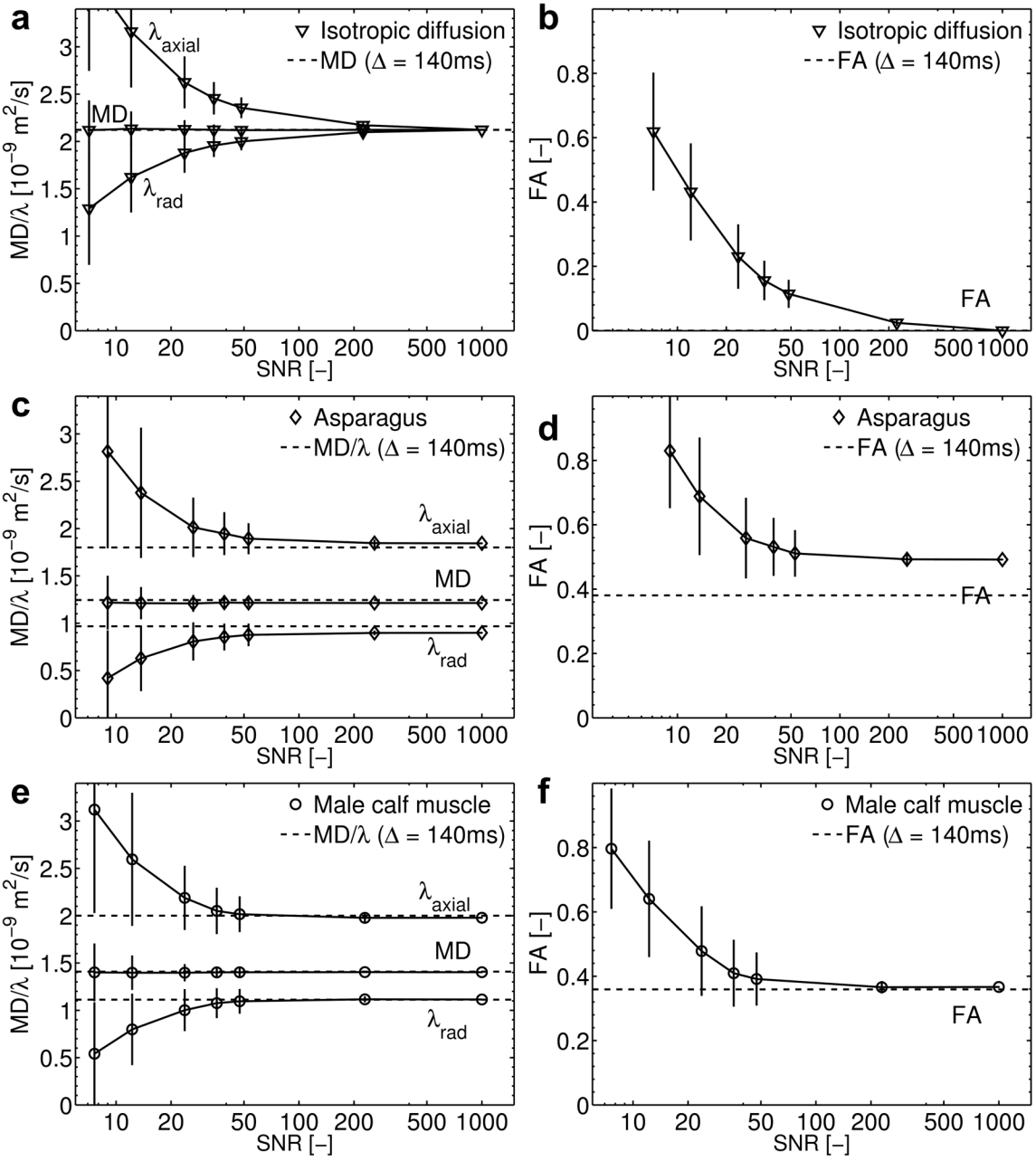

Figure 3.

Simulations of the impact of time-dependent diffusion and noise on diffusion parameters as would be measured with the MEDITATE sequence (2 series of 13 echoes): Mean Diffusivity (MD)/Eigenvalues (λ_{axial} and λ_{radial}) and Fractional Anisotropy (FA) as a function of measurement SNR of a,b) an isotropic medium (water), c,d) an anisotropic medium (asparagus stalks) [46] and e,f) *in vivo* (male) calf muscle [8,45]. The derived apparent diffusion parameters (mean and standard deviation calculated from 400 samples) are compared to input diffusion parameters (MD and FA) at a diffusion time of 140 ms (dashed lines).

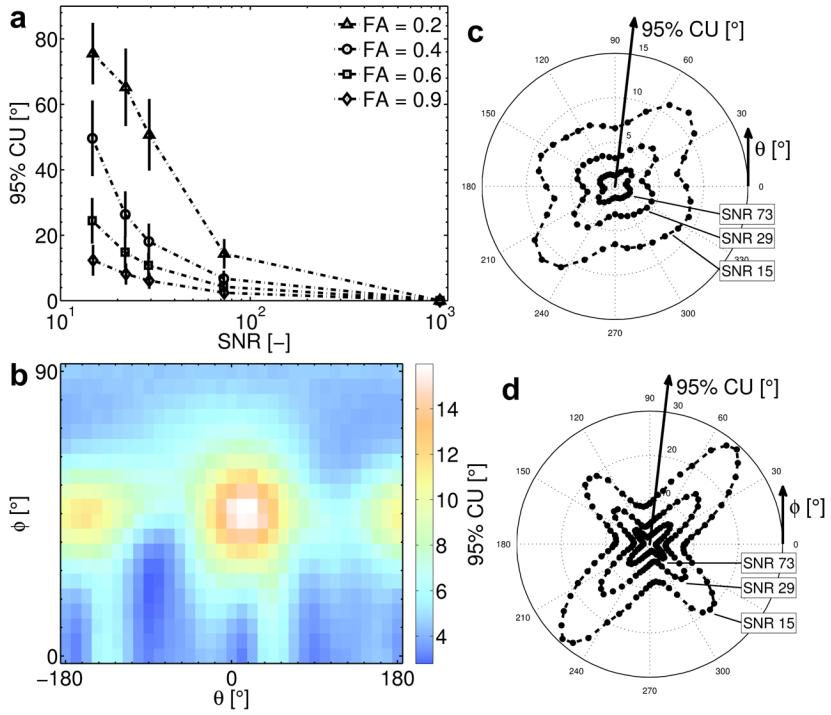

Figure 4.

Simulations of the directional variance of the diffusion encoding scheme of the MEDITATE sequence (2 series of 13 echoes): 95% confidence angles or cone of uncertainty [47] a) averaged over all tensor orientations as a function of measurement SNR and FA; b,c,d) as a function of the azimuth and elevation angles (θ and ϕ) of the tensor (FA = 0.9, MD = 1.5 10^{-9} m^2/s) in surface (c, SNR = 29) and polar plots (b,d). 95% cones of uncertainty are taken as the 95% percentile over 5000 samples for each tensor orientation.

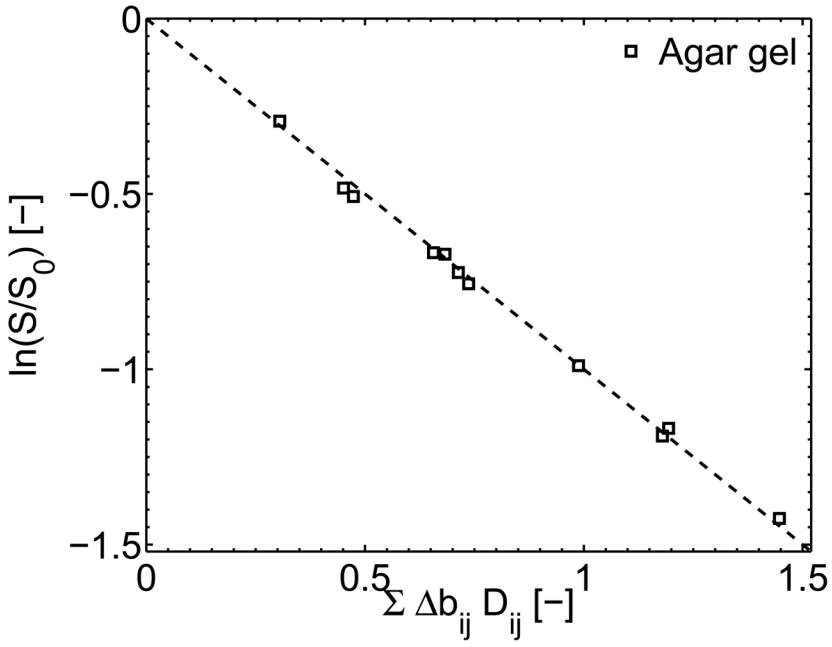

Figure 5.
The amplitude ratios of the weighted and unweighted signal of the isotropic diffusion in an agar gel sample as measured with a two dataset 5 RF-pulse MEDITATE sequence plotted versus the full diffusion weighting argument.

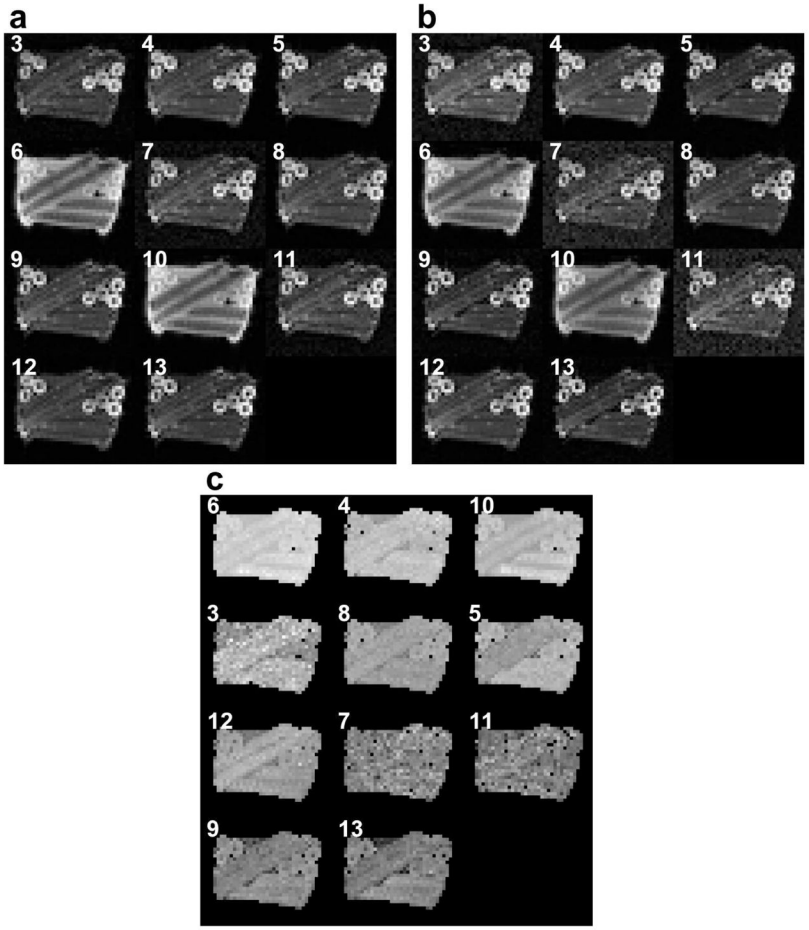

Figure 6.

Raw images of the 13 last echoes in a MEDITATE sequence with 5 RF-pulses of an anisotropic phantom (asparagus stalks in agar gel) depicted and labeled in order of increasing echo time TE. The mean isotropic b-value $\overline{(b_{xx,Q}+b_{yy,Q}+b_{zz,Q})}$ is 50 s/mm^2 in the reference scan (a) and 500 s/mm^2 in the diffusion weighted scan (b). The ratios of (b) and (a) are shown in (c) in order of increasing isotropic b-value.

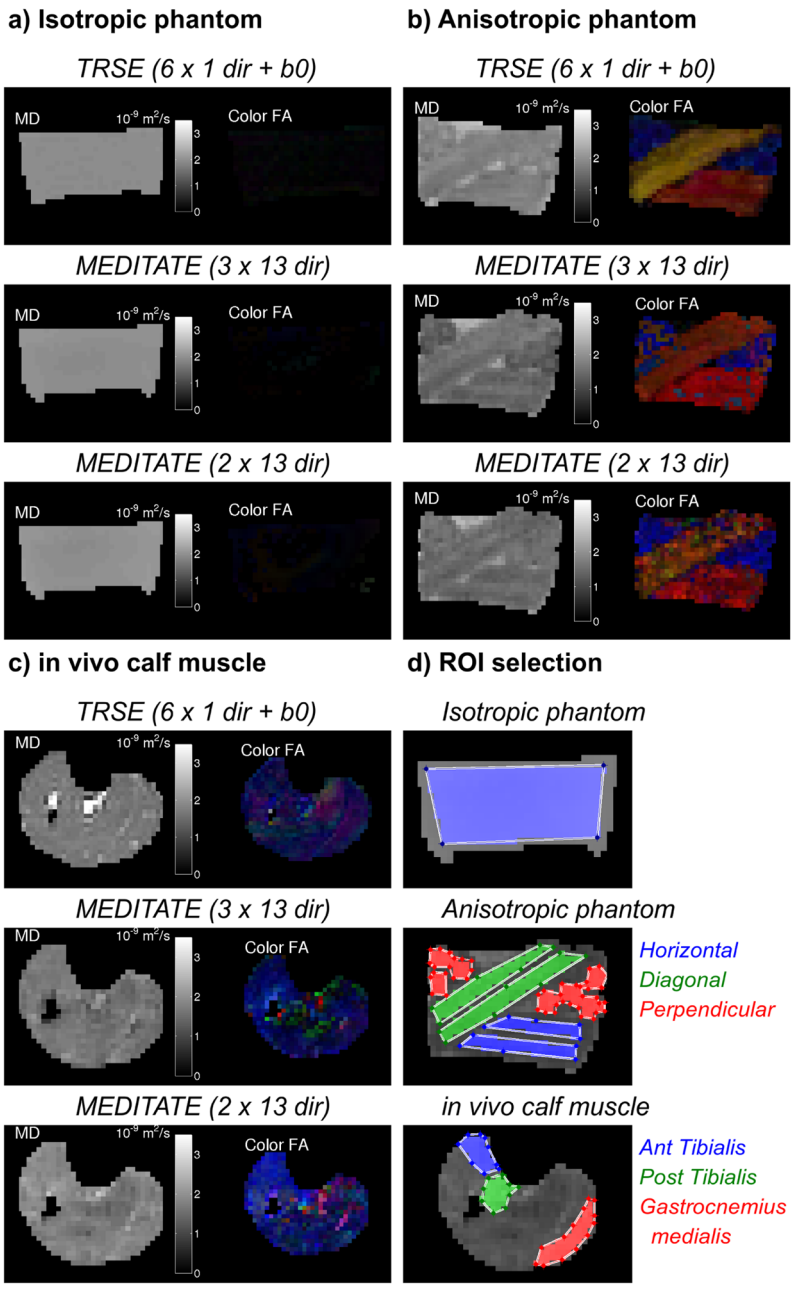

Figure 7.

Diffusion tensor parameter maps of the Mean Diffusivity (MD) and Color coded Fractional Anisotropy (Color FA; Red left-right, green anterior-posterior, blue superior-inferior) of an isotropic phantom (a), an anisotropic phantom (b) and *in vivo* healthy calf muscle of one volunteer (c). DTI-analysis was performed on images obtained with a TRSE-sequence (6 directions + b_0) and the MEDITATE sequence (3 and 2 series of 13 directions, one series is a reference series). (d) ROIs used for further analysis (Figure 9).

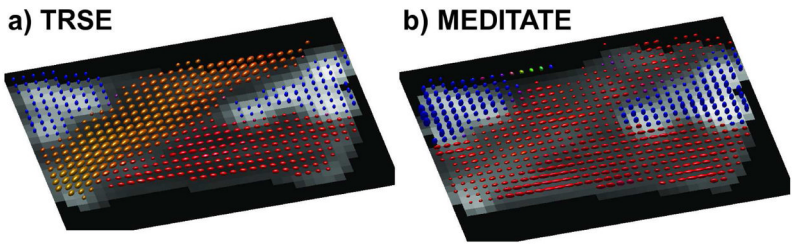

Figure 8.
Ellipsoidal visualization of the diffusion tensors of an anisotropic phantom superimposed on a b_0-image. DTI-analysis was performed on images obtained with (a) a TRSE-sequence (6 directions + b_0) and (b) the MEDITATE sequence (2 series of 13 directions, one series is a reference series).

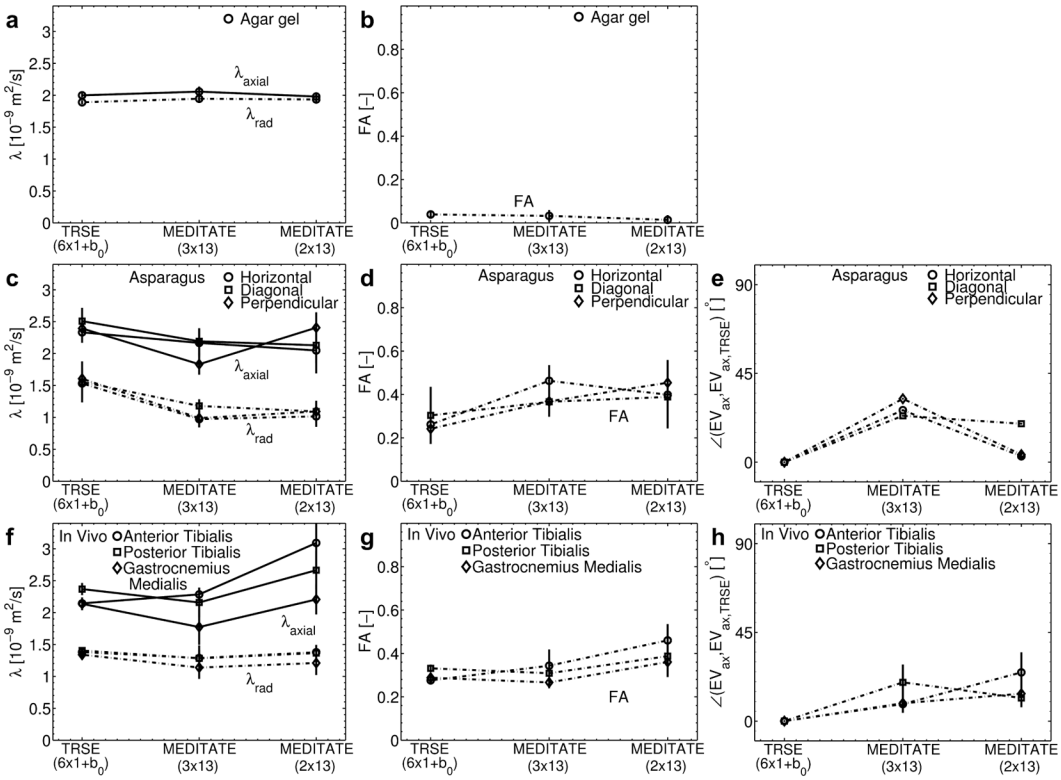

Figure 9.

Comparison of the eigenvalues (λ_{axial} and λ_{radial}), Fractional Anisotropy (FA) and the axial diffusion direction (difference angle with the axial eigenvector estimated with the TRSE-sequence) of an isotropic phantom (agar gel) (a,b), an anisotropic phantom (asparagus stalks in horizontal and diagonal in-plane and perpendicular out-of-plane directions) (c,d,e) and *in vivo* calf muscle (5 volunteers; f,g,h) sampled over a ROI in DTI parameter maps obtained from a TRSE-sequence (6 directions + b_0) and the MEDITATE sequence (3 and 2 series of 13 directions, one series is a reference series) (Example ROIs illustrated in Figure 7d). Phantom eigenvalues and FA are displayed as the mean and standard deviation of values taken from ROIs in the same phantom; the phantom diffusion direction is calculated using the mean axial eigenvector of ROIs. The *in vivo* results are the mean and standard deviation of DTI parameters across all 5 subjects in the designated ROI.

Table 1

Coherence pathways Q of the MEDITATE method described here with $N = 5$ RF-pulses. $\mu(t)$, the instantaneous value of the magnetization state of Q, is piecewise constant with values μ_j in the interval between the RF-pulses j and $j + 1$, where μ_j can be 0, +1 or −1 for the three states of spin magnetization of an ensemble of spin-1/2 nuclei $M_0 = M_Z$, $M_+ = (M_x + iM_y)/\sqrt{2}$ and $M_- = (M_x - iM_y)/\sqrt{2}$. When $N > 5$, the last four coherence pathways are repeated with $\{\mu_3 \cdots \mu_{N-1}\ \mu_N\} = \{0 \cdots 0\ -1\}$.

Echo Number	Q = $\{\mu_0\ \mu_1\ \mu_2\ \mu_3 \cdots \mu_N\}$					
	μ_0	μ_1	μ_2	μ_3	μ_4	μ_5
1	0	1	−1			
2	0	1	0	−1		
3	0	−1	1	−1		
4	0	0	1	−1		
5	0	1	1	−1		
6	0	1	0	0	−1	
7	0	−1	1	0	−1	
8	0	0	1	0	−1	
9	0	1	1	0	−1	
10	0	1	0	0	0	−1
11	0	−1	1	0	0	−1
12	0	0	1	0	0	−1
13	0	1	1	0	0	−1

Table 2

Pulse sequence parameters of the MEDITATE sequence (3 and 2 datasets of 13 directions, that is, two or one diffusion weighted datasets and one reference dataset) with timing parameters τ_1 = 9.0 ms and τ_G = 18.0 ms and echo times TE = 18.0–245.2 ms. In each combination, the first diffusion gradient set is used for the reference dataset.

datasets	b_{iso} [s/mm^2]	cond(B) [−]	Diffusion gradient moments [mT/m·ms]		
			$\vec{G_1}$	$\vec{G_2}$	$\vec{G_3}$
3	8–810	3.77	(−16,−11,−10)	(−11,11,11)	(193,−66,−35)
			(−66,60,−97)	(88,124,−98)	(−35,−22,−87)
			(−63,−88,32)	(97,−83,−65)	(142,−58,−135)
			$\vec{G_4}$	$\vec{G_5}$	$\vec{G_6}$
			(9,−33,110)	(108,131,−6)	(−20,−10,−25)
			(−61,−428,259)	(284,142,−349)	(261,263,−256)
			(−14,−366,−10)	(35,−33,−22)	(86,−264,−23)
			$\vec{G_1}$	$\vec{G_2}$	$\vec{G_3}$
2	10–790	4.42	(−15, −29,14)	(28, −11, −46)	(−6,250,30)
			(−52, −110,58)	(87, −94, −96)	(−367,229, −312)
			$\vec{G_4}$	$\vec{G_5}$	$\vec{G_6}$
			(−60,62,135)	(−30, −77,10)	(−221,119,44)
			(315, −32,217)	(22, −313, −184)	(228, −296, −315)